Closed-Loop Control of DC–DC Dual-Active-Bridge Converters Driving Single-Phase Inverters

Hengsi Qin, *Member, IEEE*, and Jonathan W. Kimball, *Senior Member, IEEE*

***Abstract*—A solid-state transformer (SST) is a high-frequency power electronic converter that is used as a distribution power transformer. A common three-stage configuration of an SST consists of ac–dc rectifier, isolated dc–dc dual-active-bridge (DAB) converter, and dc–ac inverter. This study addresses the controller design issue for a dc–dc DAB converter when driving a regulated single-phase dc–ac inverter. Since the switching frequency of the inverter stage is much higher than that of the DAB stage, the single-phase inverter is modeled as a double-line-frequency (e.g., 120 Hz) current sink. The effect of 120-Hz current by the single-phase inverter is studied. The limitation of a PI-controller, low gain at 120 Hz, is investigated. Two methods are proposed to improve the regulation of the output voltage of DAB converters. The first one uses a bandstop filter and feedforward, while the second method uses an additional proportional-resonant controller in the feedback loop. Theoretical analysis, simulation, and experiment results are provided.**

***Index Terms*—DC-DC power converters, pulse width modulation converters, power smoothing.**

I. Introduction

THE multistage ac–dc–ac–dc–ac configuration shown in Fig. 1 is one of many feasible single-phase SST topologies [1]–[4]. An SST is used to interface between a medium-voltage distribution network (e.g., 7.2 kV) and a low-voltage distribution network (e.g., 240 V). The output voltage and the output current of the inverter stage are grid frequency, while the input and output voltages of the dual-active-bridge (DAB) converter stage are dc. As a result, the instantaneous output power fluctuates at twice the line frequency and there is significant second-order harmonic current at the input side of the inverter stage. When a dc–dc DAB converter is driving such an inverter, it is common to select a sufficiently large output capacitor bank to absorb the double-frequency harmonic current and to minimize the output voltage ripple. Because the second-order harmonic frequency is relatively low, this might result in a large capacitor bank at the output side of the DAB converter, which increases cost, weight, and volume. Furthermore, large electrolytic capacitors are one major factor affecting the reliability of power converters. For the remainder of this study, line frequency is assumed to be 60 Hz, so the ripple current in the output capacitor is at 120 Hz.

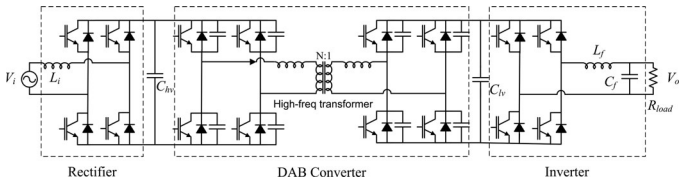

Fig. 1. Circuit configuration of multistage SSTs.

One way to reduce the output capacitor bank is to enable dc–dc DAB converters with the ability to process power at 120 Hz. As a result, both average power and 120 Hz power are processed by the rectifier, DAB converter, and inverter, from the grid to the load. However, the control bandwidth is limited and the loop gain at 120 Hz is limited because the switching frequency of DAB converters is constrained by the availability of power devices [3]. When a conventional PI controller is used, it only achieves infinite gain at dc. Small, finite gain leads to nonzero steady-state error at 120 Hz, resulting in high voltage ripple at the output of DAB converters.

This study addresses such limitations of a conventional PI controller for a dc–dc DAB converter driving a single-phase dc–ac inverter. Two methods are proposed to solve this issue. The first one adds an additional feedforward path to a conventional PI controller. The second method uses a proportional-integral-resonant (PI-R) controller, which achieves high gain at 120 Hz.

A PR controller is able to achieve infinite gain at a given frequency. PR controllers in a stationary frame are equivalent to PI controllers in a d-q rotational frame, as proven in [5] and [6]. A PR controller is suitable for single phase ac applications because power in single phase systems is fluctuating at 120 Hz (the second-order harmonic) [7], [8]. A PR controller is also used in three-phase inverters to achieve zero steady-state error and to compensate voltage harmonics and/or unbalanced contents caused by nonlinear loads, without using the time-consuming coordinate transformations [7], [9]–[11]. PR controllers have been applied to single-phase active rectifiers [12], grid-tie inverters [13], UPS [14], distributed power generation [15], and dynamic voltage restorers (DVRs) [16]. A comprehensive review of PR controllers for a single-phase dc–ac inverters is presented in [7]. The sensitivity of PR-controlled single-phase inverters is discussed in [17]. Impedance matching of a PR-controlled inverter is addressed in [18], and the implementation of PR controllers in the form of digital filters is discussed in [19] and [20]. The common theme in all of these prior works is the control of ac-side quantities, usually in a three-phase system, without the need for a reference frame conversion. This study

Manuscript received October 24, 2012; revised January 31, 2013 and March 13, 2013; accepted March 14, 2013. Date of current version August 20, 2013. Recommended for publication by Associate Editor R. Burgos.

H. Qin is with the SolarBridge Technologies, Inc., Austin, TX 78758 USA (e-mail: hengsi.qin@mail.mst.edu).

J. W. Kimball is with the Missouri University of Science and Technology, Rolla, MO 65409 USA (e-mail: kimballjw@mst.edu).

Color versions of one or more of the figures in this paper are available online at http://ieeexplore.ieee.org.

Digital Object Identifier 10.1109/TPEL.2013.2257859

incorporates the PR concept within a PI controller to account for both dc and ac components on the dc side of the inverter.

A few of these prior works deserve special mention. The study in [7] explored various combinations of proportional, integral, derivative, resonant, and load current feedback terms for the control of a single-phase inverter, along with a d-q frame controller. Broadly, the conclusion is that P+R control has the best steady-state performance, which motivated this study. In [8], which addresses an unusual boost-converter-based single-phase inverter, the internal model principle is cited as the primary reason to include a PR term, and indeed the converter achieves its objectives. The various PR controllers in [9], [10], and [12] address harmonics in three-phase inverters. As compared to a synchronous-frame d-q controller, a PR controller can handle both positive and negative sequence components at a given frequency, thereby reducing the need for reference frame conversions. All of these papers, though, address inverters, whereas this study addresses a dc–dc converter with an oscillating load. Finally, in [17], Nyquist methods are used to study stability for cases where the resonant term gives rise to multiple crossings of 0 dB. In such cases, Bode methods are no longer useful. However, in this study, the 0 dB crossing occurs beyond the resonant frequency, so Bode methods are still effective in evaluating stability.

In some converter types, feedforward is easier to implement with current mode control. That is, rather than controlling the duty ratio, the current is controlled directly, so a double-frequency component may be added to the current reference. In the DAB, current mode is rarely used. Indeed, all of the methods compared in [21] are different types of pulse width modulation (PWM) that are used to improve the efficiency of the DAB, while retaining the general modulation principles used here. Implementing current control requires a PI loop (or equivalent controller) as used in [22]. Most other recent innovations focus on extending the soft-switching range or making the converter more robust to parameter changes, such as [23]–[26].

This paper is organized as follows. Section II discusses the model approximation in this study. Section III uses the average models of DAB converters to discuss the limitation of conventional PI controllers. Section IV presents two solutions: 1) a feedforward path added to a conventional PI controller and 2) a novel PI-R controller. It studies the dynamics in frequency domain to show the advantages of a PI-R controller for DAB converters. Section V presents the simulation and experimental results to verify the proposed control strategy. Section VI summaries the contribution of this study .

II. System Configuration and Approximation

Without loss of generality, this study lumps the series–paralleled rectifiers and DAB converters, as commonly used to achieve high voltage ratings for a distribution-level SST, into one equivalent rectifier and one equivalent DAB converter, respectively. The schematic of a single-phase SST is shown in Fig. 1. The first stage is a single-phase active front-end rectifier, which converts the grid ac voltage to a fixed dc voltage. The second stage is an isolated dc–dc DAB converter, which transfers

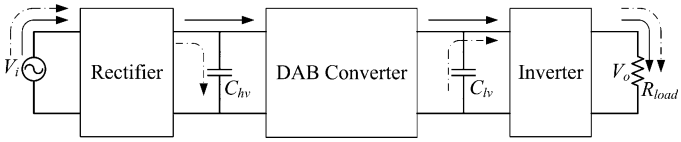

Fig. 2. Conventional power flow of multistage SSTs. Solid lines indicate average power and dashed lines indicate double-frequency power ripple.

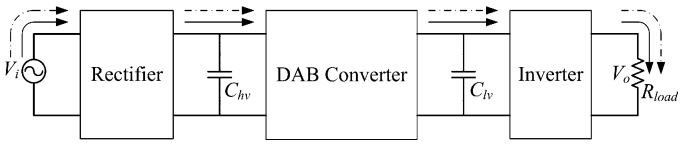

Fig. 3. Novel power flow of multistage SSTs. Solid lines indicate average power and dashed lines indicate double-frequency power ripple.

power between two dc buses with a high-frequency transformer. The "output" dc bus is defined as the bus whose voltage is regulated by the DAB converter, which is the low-voltage bus on the right in Fig. 1. The last stage is a single-phase dc–ac inverter, which generates an ac sinusoidal voltage as the SST's output voltage.

The conventional power flow diagram of a multistage SST is given in Fig. 2. Ideally, the voltage and current at both the input of the rectifier and the output of the inverter are line frequency, e.g., 60 Hz. Therefore, the input power of the rectifier and the output power of the inverter consist mainly of average power (which is in dc) and ripple power (which is the second-order harmonic content at 120 Hz).

$$P = \sqrt{2}V\sin(\omega_s t)\sqrt{2}I\sin(\omega_s t) = VI\left(1+\cos\left(2\omega_s t\right)\right) \quad (1)$$

where V represents input/output RMS voltage, I represents input/output RMS current, $\omega_s = 2\pi f_s$, and $f_s = 60$ Hz is the grid frequency. On the other hand, the conventional control method for a dc–dc DAB converter can only process dc power. This means that the two dc buses must absorb the 120 Hz ripple power, as visualized in Fig. 2 (solid lines represent dc power while dash lines represent 120 Hz ripple power). Because 120 Hz is a relatively low frequency, large bus capacitance is needed to reduce the bus voltage fluctuation and achieve sufficiently high ripple current ratings.

The novel power flow diagram of a multistage SST is given in Fig. 3. Once the DAB converter is capable of processing power at 120 Hz, both average power and 120 Hz ripple power are transferred from the input port to the output port, which reduces the requirement for the capacitance on the two dc buses. This is advantageous because less capacitance means lower component cost and higher reliability.

Because the focus of this study is on the DAB converters in SSTs, the following assumptions are made: 1) the rectifier stage has been well designed to provide a stable input dc voltage for the DAB stage; 2) the inverter stage has been well designed to provide a 120 V sinusoidal output voltage at 60 Hz; and 3) the switching frequency of the inverter is higher than that of the DAB converter and the switching frequencies of all converter stages are much higher than the grid frequency. In this study, the switching frequencies of the DAB converter and the inverter

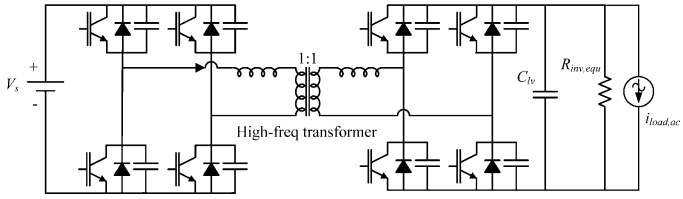

Fig. 4. Simplified schematic of a DAB converter driving an inverter.

are set to 5 and 20 kHz, respectively. Because the DAB input voltage is much higher than the inverter input voltage for an SST at the distribution level [1], lower switching frequency of the DAB converter is required. Using these assumptions, the active front-end rectifier is replaced by a constant voltage source. The inverter, as the load of DAB converter, is modeled as a variable resistor consisting of two parts, one at dc and one varying at 120 Hz.

Using the first assumption above, the active front-end rectifier is replaced by a constant voltage source. As mentioned before, the switching frequency of the DAB converter is lower than that of the inverter because of limited device switching performance. The input current of the inverter contains mainly dc and second-order harmonic contents. Furthermore, the switching frequencies of both DAB converter and inverter (5 kHz and 20 kHz, respectively) are significantly higher than the grid frequency and its second-order harmonic frequency (60 and 120 Hz, respectively). Therefore, the quasi-steady-state inverter model is valid. The inverter, as the load of the DAB converter, is modeled here as a resistor in parallel with an ac current source with a frequency of 120 Hz. More detailed models are available, such as [27], but the Norton load model is sufficient for the purposes of controller design. The simplified system schematic is shown in Fig. 4. The control method used here and analyzed in [28] sets the duty ratio of each bridge of the DAB to approximately 50% (with some deadtime for zero voltage switching) and controls the power flow with the phase angle between the two bridges. The phase angle becomes an equivalent duty ratio d in the analysis below.

III. Model Analysis

After the approximation, the problem becomes how to model a dc–dc DAB converter. Instead of using the simplified reduced-order continuous-time model in [29]–[31] or the full-order discrete-time model in [32] and [33], this study uses the full-order continuous-time model derived in [28] using the generalized average modeling technique. The proposed model is able to provide a more accurate control-to-output transfer function. For convenience, the small-signal control-to-output transfer function given in [28] is repeated below in the matrix form

$$\frac{d}{dt}x = Ax + B\Delta d \tag{2}$$

$$y = Cx \tag{3}$$

where

$$x = [\,\Delta v_{o0} \quad \Delta i_{t1R} \quad \Delta i_{t1I}\,]^T \tag{4}$$

TABLE I
Circuit Parameters of the DAB Converter

Inductance, input side	500 μH
Inductance, LV	500 μH
Switch Frequency	5 kHz
ZVS Capacitor	2.7 nF
Output Capacitor	200 μF
Switching Device	ST STD8NM60ND 600V 7.3A MOSFET

TABLE II
Transformer Design of the DAB Converter

Core Type	Ferrite ETD 54
Core Area	3.55 cm^2
Window Area	3.16 cm^2
Area Product	8.85 cm^4
wire, input side	108 turns AWG 20
wire, output side	108 turns AWG 20
MMF Layout	Input: 3 portions, 1 layer/portion Output: 3 portions, 1 layer/portion

$$y = [\,\Delta v_{o0}\,], \tag{5}$$

$$A = \begin{bmatrix} -\dfrac{1}{RC_o} & -\dfrac{4\sin(D\pi)}{\pi C_o} & -\dfrac{4\cos(D\pi)}{\pi C_o} \\ \dfrac{2\sin(D\pi)}{\pi L_t} & -\dfrac{R_t}{L_t} & \omega_s \\ \dfrac{2\cos(D\pi)}{\pi L_t} & -\omega_s & -\dfrac{R_t}{L_t} \end{bmatrix} \tag{6}$$

$$B = \begin{bmatrix} \dfrac{4}{C_o}\left(I_{0I}\sin(\pi D) - I_{0R}\cos(\pi D)\right) \\ \dfrac{2V_{o0}}{L_t}\cos(\pi D) \\ -\dfrac{2V_{o0}}{L_t}\sin(\pi D) \end{bmatrix} \tag{7}$$

and

$$C = [\,1 \quad 0 \quad 0\,]^T. \tag{8}$$

In (2)–(8), v_{o0} is the output voltage of the DAB converter; i_{1R} and i_{1I} are the real part and imaginary part of the transformer current of the DAB converter, respectively; $R = \frac{V_o^2}{P}$ is the equivalent small-signal input impedance of the inverter at nominal load; C_o is the output capacitance of the DAB converter; L_t is the transformer leakage inductance of the DAB converter; R_t is the lumped equivalent series resistance of transformer windings; $\omega_s = 2\pi f_s$ and $f_s = 5000$ Hz is the switching frequency of DAB converter; and d is the phase-shift ratio between the two bridges of the DAB converter. Variables in capital letters represent nominal values, while those in lower case letters represent small-signal variables.

The control-to-output transfer function of a DAB converter is given by

$$G_{vd}(s) = C\left(sI - A\right)^{-1}B. \tag{9}$$

Given the circuit parameters described in Tables I, II, and III, Fig. 5 shows the control-to-output transfer function of a DAB

TABLE III
CIRCUIT PARAMETERS OF AN INVERTER

Filter inductance	300 μH
Filter capacitance	30 μF
Switch Frequency	20 kHz
Rated Load Resistance	36 Ω
Switching Device	ST STGD3HF60HD 600V 7A IGBT

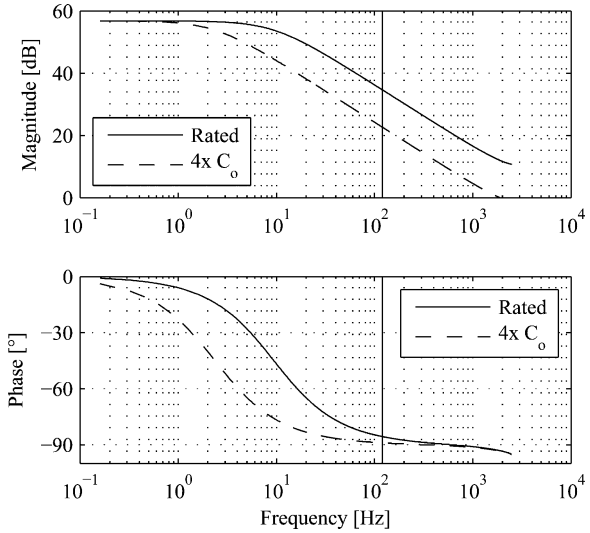

Fig. 5. DAB control-to-output transfer function, with nominal and four times output capacitance (Vertical line marks 120 Hz).

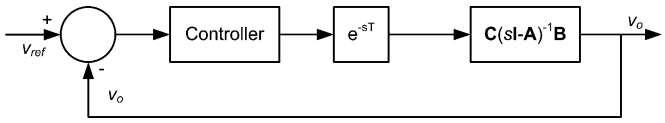

Fig. 6. Small-signal schematic of the closed-loop controlled DAB converter.

converter driving a variable inverter-equivalent load. Also included in Fig. 5 is the transfer function with four times the output capacitance, representing the hardware solution to the output voltage ripple problem.

The power transferred by a DAB converter is given by

$$P = \frac{v_s v_o}{2 f_s L_t} d\,(1-d) \tag{10}$$

where v_s is the input voltage. Given a specified power rating, a range of preferred phase-shift ratio d, and a specific range of soft switching, the product of transformer leakage inductance L_t, and switching frequency f_s is fixed. Therefore, increase of f_s would result in decrease of L_t, canceling the effect of increasing switching frequency. Only output capacitance significantly affects the transfer function of the converter, as shown in Fig. 5.

For a well designed inverter, there is a significant 120 Hz harmonic current at the input side of the inverter. This harmonic current poses a design challenge to the DAB converter, caused by limited control bandwidth of the DAB converter. Fig. 6 shows the small-signal schematic of a closed-loop feedback control system that consists of a DAB converter and a PI controller (as shown in Fig. 7). Note that a delay term e^{-sT_d} is added to the

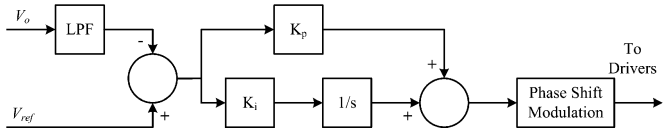

Fig. 7. Diagram of PI-only control.

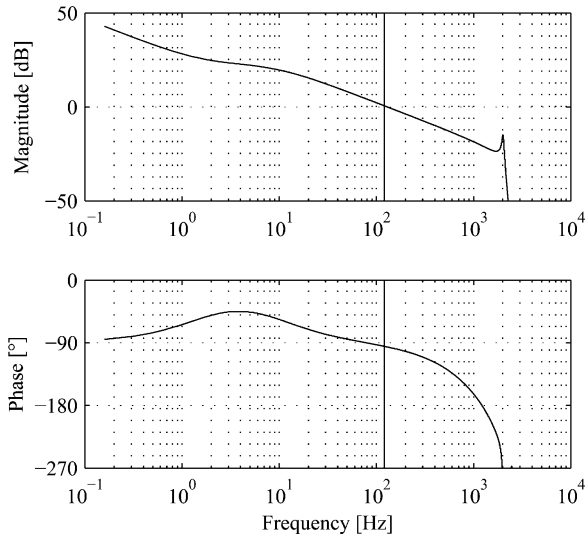

Fig. 8. Bode plot of PI-only method (Vertical line marks 120 Hz).

feedback loop in Fig. 6 to represent the sampling and processing delay T_d, which is caused by the digital implementation of the control algorithm and modulation processes. In the present example, the switching frequency f_s is 5 kHz, so $T_d = 200\,\mu$s. As a result, the loop gain has significant phase delay at frequencies approaching f_s, which limits the possible bandwidth.

Since the DAB converter has one dominant pole according to Fig. 5, a single PI controller seems a candidate solution because of simplicity. Fig. 7 shows the structure of a PI controller. Fig. 8 shows the bode plot of the loop gain of a dc–dc DAB converter with a PI controller. The gain around 120 Hz (753 rad/s) is low, which indicates that it is difficult to track and compensate the disturbance caused by the 120 Hz harmonic current from an inverter. One possible solution is to increase the gain K_p of the PI controller. However, as shown in Fig. 9, a high-gain PI controller would decrease phase margin (here only $44.7°$) and might even destabilize the control loop. In simulation studies, the gain may be increased from the base case by approximately a factor of two before extra harmonics begin appearing in the bus voltage (240 Hz rather than 120 Hz). The ripple only decreases by about 30%, though, trading a significant reduction in stability margin for a modest improvement in ripple. A larger output capacitor is preferred in order to increase phase margin and improve stability, which, however, results in lower gain at 120 Hz and cancels the effect of increasing controller gain.

A PI controller is not the optimal control solution for a DAB converter driving an inverter because of low gain around 120 Hz. Therefore, two improvements over PI-only control will be introduced.

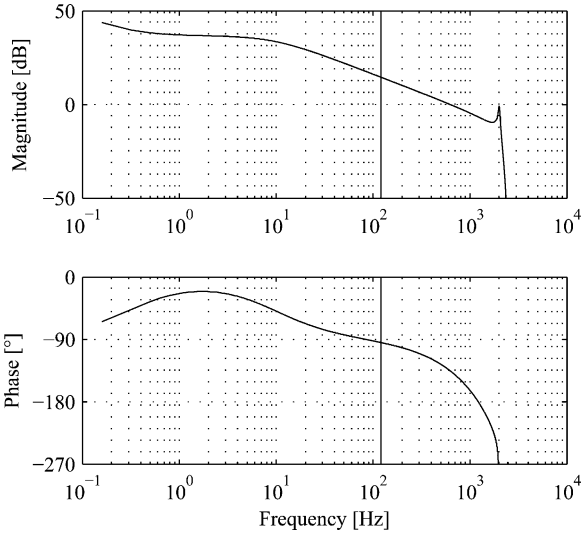

Fig. 9. Bode plot of PI-only method with higher proportional gain (Vertical line marks 120 Hz).

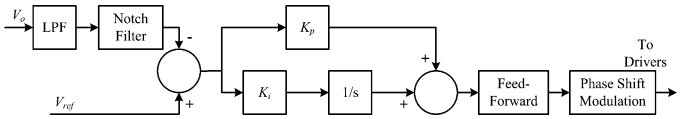

Fig. 10. Diagram of PI plus feedforward control.

IV. Two Proposed Solutions

The control target of a DAB converter driving an inverter consists of two parts:1) regulate output dc voltage and control the average output power and 2) suppress the 120 Hz disturbance from the inverter and track the 120 Hz ripple power. PI-only control can only meet the first target and fails to meet the second target. Two methods are proposed to address the control challenge caused by low gain at 120 Hz of the feedback loop with only a PI controller. The first method adds a feedforward path to the existing PI controller, while the second one uses an additional resonant controller to form a PI-R control. These two methods will be discussed in detail as follows.

A. Method 1—PI Plus Feedforward Control:

The first method is a PI controller assisted by an additional direct feedforward portion. Fig. 10 shows the schematic of the proposed control method. In Fig. 10, the PI controller only takes care of the first control target, output dc voltage, while the feedforward portion is responsible for tracking the 120 Hz fluctuating power.

After sampling the output voltage of the DAB converter, instead of using an antialiasing filter, this method uses a low-pass filter (LPF) whose passband is below 120 Hz. As a result, the 120 Hz content in the sampled signal is suppressed by the LPF. The feedback signal fed into the PI controller is essentially dc. Therefore, the PI controller shown in Fig. 10 is called the dc regulator. Because the LPF has a low cut-off frequency and the PI controller only regulates dc voltage, the bandwidth of the PI

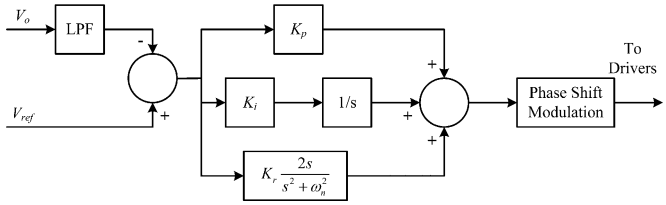

Fig. 11. Diagram of PI-R control.

controller does not need to be high and it is called low-bandwidth PI controller.

The feedforward portion is introduced in order to track the 120 Hz ripple power generated by the inverter. In this study, the inverter and the DAB converter share a single DSP unit as controller. The phase angle of inverter's output voltage is set by the controller of an inverter. Therefore, such a phase angle is also known to the controller of the DAB converter. From (1), the power angle in a 120 Hz cycle (θ_p) can be calculated from the output voltage's phase angle (θ_v) as

$$\theta_p = 2\theta_v - \frac{\pi}{2}. \tag{11}$$

The sinusoidal feedforward signal in (11) is at 120 Hz and is used to compensate the second-order harmonic content.

The feedforward solution preserves the large-signal dynamics of the original PI controller and provides excellent ripple rejection for unity power factor loads. However, performance suffers for lower power factor loads. Therefore, a closed-loop controller combining a PI controller with a resonant controller is introduced next.

B. Method 2—PI-R Control:

To compensate for the 120 Hz power fluctuation, the feedback compensator must have high gain around that frequency. Increasing the gain of the PI controller might meet this goal, but at the expense of reduced phase margin. This study develops a new compensator based on the PI-resonant (PI-R) scheme, in which the PI portion regulates the dc output voltage and the resonant portion directly compensates for the 120 Hz ripple voltage. The schematic diagram of the proposed controller is shown in Fig. 11. Such controller, instead of using any feedforward from the inverter, adds an additional resonant controller (R controller) in parallel with the existing PI controller.

An R controller is known for its equivalence to a PI controller in the synchronously rotating reference frames [7], [9]–[11]. It is able to obtain zero steady-state error for a sinusoidal reference signal without coordinate transformation. The transfer function of R-controller is

$$G_{\mathrm{PR}}(s) = K_r \frac{2s}{s^2 + \omega_2^2} \tag{12}$$

where $\omega_2 = 2\pi 120$ rad/s represents the second-order harmonic frequency of grid frequency. The R controller adds two poles at 120 Hz to increase the loop gain dramatically around that frequency. Combining a PI controller with an R controller, the

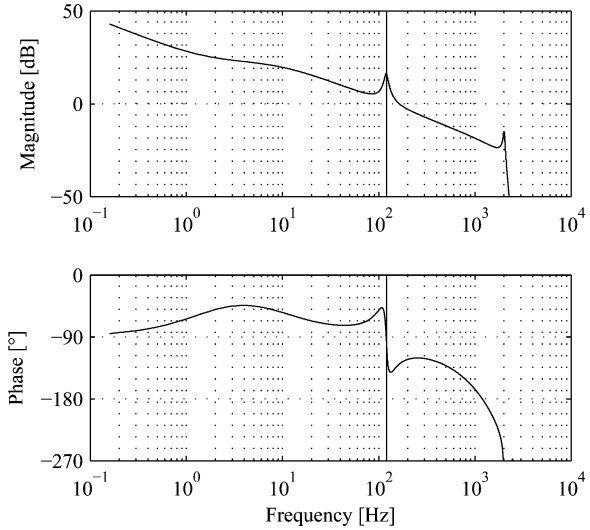

Fig. 12. Bode Plot of the PI-R Method (Vertical line marks 120 Hz).

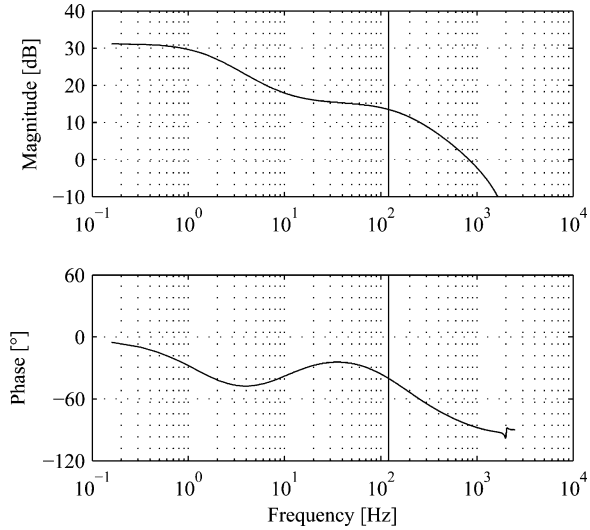

Fig. 13. Output Impedance with PI-only control (Vertical line marks 120 Hz).

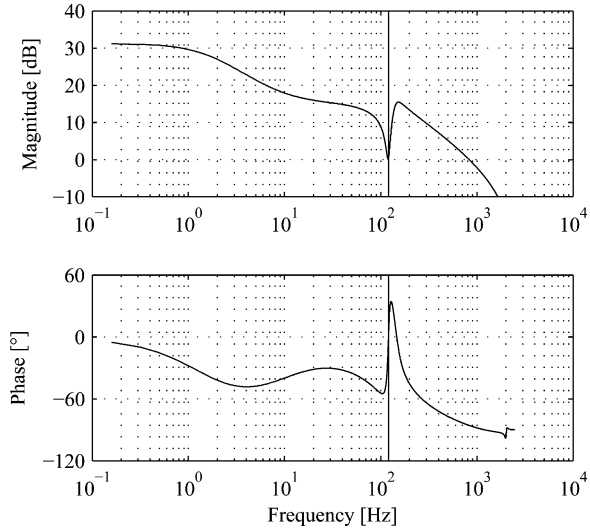

Fig. 14. Output Impedance with PI-R control (Vertical line marks 120 Hz).

transfer function of the regulator is

$$G_{\mathrm{PIR}}(s) = K_p + K_i \frac{1}{s} + K_r \frac{2s}{s^2 + \omega_2^2}. \tag{13}$$

The idea of this method is: the PI controller achieves high gain at dc while the R controller achieves high gain at the second-order harmonic frequency. Therefore, both the error at dc and the error at 120 Hz are attenuated. Because of the interaction between the PI portion and the R controller, the combined controller has three poles and three zeroes, preserving phase characteristics far from 120 Hz but increasing the order of the system and corresponding dynamic characteristics.

If an output voltage reference v_{ref} is considered as reference and an inverter input current i_{inv} is considered as disturbance, the output voltage v_o in the frequency domain can be expressed as

$$v_o(s) = v_{\mathrm{ref}}(s) \cdot G_1(s) + i_{\mathrm{inv}} \cdot G_2(s) \tag{14}$$

where

$$G_1(s) = \frac{G_{\mathrm{PIR}}(s) \cdot G_{vd}(s)}{1 + G_{\mathrm{PIR}}(s) \cdot G_{vd}(s)} \tag{15}$$

$$G_2(s) = \frac{\frac{1}{sC_o}}{1 + G_{\mathrm{PIR}}(s) \cdot G_{vd}(s)} \tag{16}$$

and $v_{\mathrm{ref}}(s), i_{\mathrm{inv}}(s)$, and $v_o(s)$ are variables $v_{\mathrm{ref}}, i_{\mathrm{inv}}$ and v_o in the Laplace domain.

In (14), $v_{\mathrm{ref}}(s)$ is dc while $i_{\mathrm{inv}}(s)$ contains mainly dc and second-order harmonic contents generated by an inverter. Therefore, the steady-state value of (14) is

$$v_o = v_{\mathrm{ref}} \cdot 1 + i_{\mathrm{inv}} \cdot 0 = v_{\mathrm{ref}} \tag{17}$$

if $K_i \cdot K_p \cdot K_r \neq 0$, because

$$\lim_{s \to 0} G_{\mathrm{PIR}}(s) = +\infty \tag{18}$$

and

$$\lim_{s \to \omega_2} G_{\mathrm{PIR}}(s) = +\infty. \tag{19}$$

Equation (17) means that ideally, the proposed PI-R control can obtain zero steady-state error.

The Bode plot of loop gain using PI-R controller is shown in Fig. 12. The loop gain has high gain at dc and around 120 Hz. The R controller only affects the loop gain around 120 Hz, besides which the loop gain is very similar to the one shown in Fig. 8. This is an advantage of the proposed control scheme. The PI controller and the R controller can be designed separately, the first one for dc regulation and the second one for 120 Hz harmonic regulations. This means that the closed-loop feedback system with the PI-R control provides good regulation of output voltage at dc and at 120 Hz.

The effect of adding an R controller to the existing PI controller can also be analyzed using the impedance approach. The small-signal output impedance of the DAB converter is

TABLE IV
PARAMETERS OF CONTROLLERS

	β_0	β_1	β_2	α_0	α_1	α_2
PI Controller	0	0.02002	-0.01998	0	1	-1
R Controller	0.00062	0	-0.00062	1	-1.965	0.9876

TABLE V
PARAMETERS OF DIGITAL FILTERS

	0	1	2	3	4	5
LPF $f_{pass} = 1kHz$, β_i	0.754	0.2331	0.3821	0.3821	0.2331	0.754
LPF $f_{pass} = 1kHz$, α_i	1	-0.3873	0.7755	-0.0959	-0.0891	0.000307
LPF $f_{pass} = 32Hz$, β_i	0.000151	0.00106	0.00318	0.00318	0.00106	0.000151
LPF $f_{pass} = 32Hz$, α_i	1	-3.9274	7.0375	-1.8829	0.4271	-0.0424

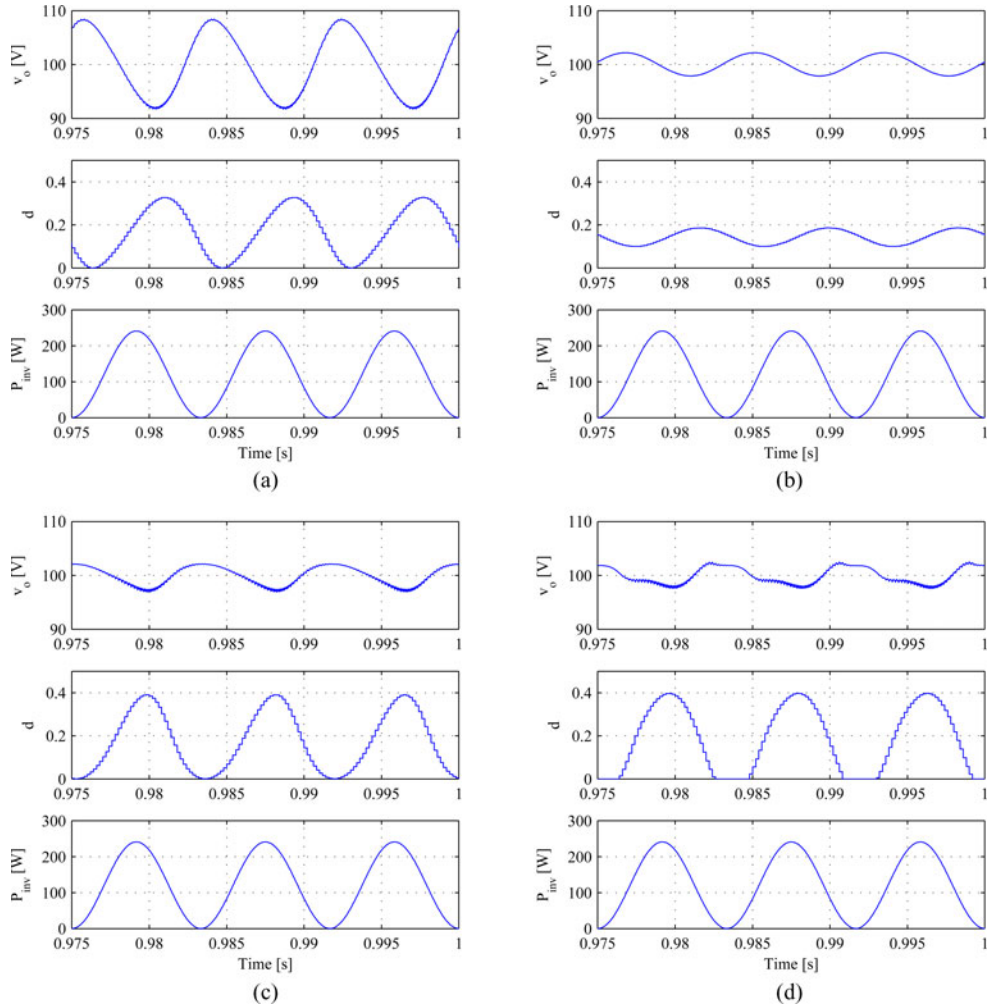

Fig. 15. Simulation Results. From top to bottom within a set: output voltage of the DAB converter (V), duty ratio of the DAB converter, output power of an inverter (W). Load is pure resistive, 30 Ω. (a) PI-only Control. (b) PI-only Control with four times capacitor. (c) PI-Feedforward Control. (d) PI-R Control.

expressed as the transfer function from the output current of the DAB converter to its output voltage,

$$Z_o = \frac{\frac{1}{sC_o}}{1 + G_{\mathrm{PIR}}(s) \cdot G_{vd}(s)}. \tag{20}$$

Figs. 13 and 14 show the Bode plot of the DAB converter's output impedance with PI-only control and PI-R control, respectively. When using the PI-R control scheme, the DAB converter has lower output impedance (by about 13 dB) around 120 Hz than the one using PI-only control. This means that lower

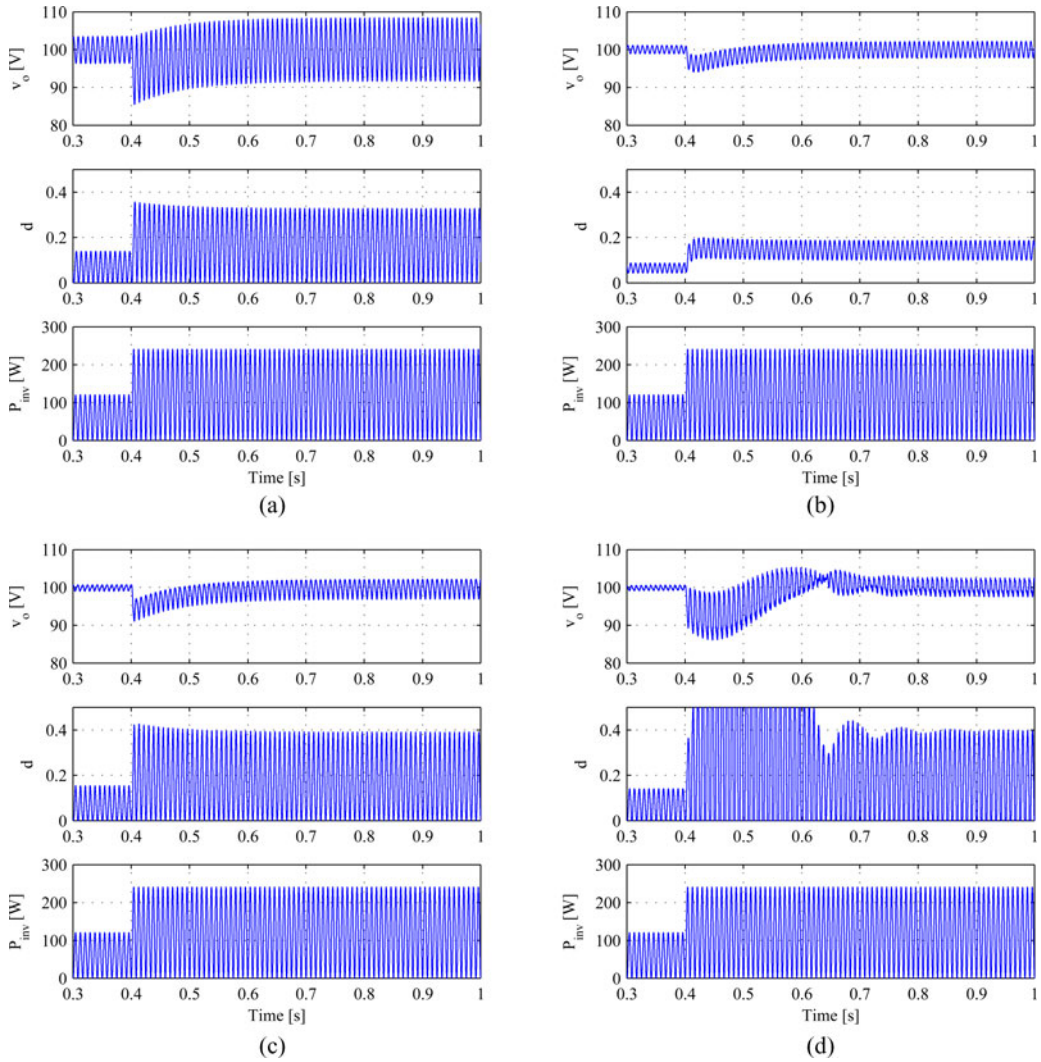

Fig. 16. Simulation Results. From top to bottom within a set: output voltage of the DAB converter (V), duty ratio of the DAB converter, output power of an inverter (W). Load is pure resistive, with a step from 60 to 30 Ω at 0.4 s. (a) PI-only Control. (b) PI-only Control with four times capacitor. (c) PI-Feedforward Control. (d) PI-R Control.

voltage ripple will be caused by the same 120 Hz ripple current when the proposed PI-R control is used.

C. Implementation in a Digital Processor

To implement the proposed control schemes digitally in a low-cost Texas Instruments floating-point DSP, TMS320F28335, the continuous-time domain transfer functions of controllers and filters must be digitized using an appropriate discrete-time conversion method. Zero-order hold (ZOH) and bilinear transformation (also known as Tustin transformation) are two well-known discretization methods [34]. Although the ZOH method is simpler, it introduces delay that affects the stability of the system, whereas the Tustin transformation preserves the stability of the original continuous-time system. Therefore, this study uses the Tustin transformation. The resulting transfer functions are parameterized as

$$G(z) = \frac{\beta_0 z^n + \beta_1 z^{n-1} + \cdots + \beta_n}{\alpha_0 z^n + \alpha_1 z^{n-1} + \cdots + \alpha_n}. \tag{21}$$

The parameters of the digitalized controller transfer functions using $K_p = 0.02, K_i = 0.2, K_r = 0.1$, and $T = 200\,\mu$s are listed in Table IV. The parameters for the antialiasing filter (for PI-only and PI-R control, sampling frequency 5 kHz, passband frequency 1.0 kHz, stopband gain -40 dB) and the LPF (for PI-Feedforward control, sampling frequency 5 kHz, passband frqunency 32 Hz, stopband gain -40 dB) are given in Table V.

V. Simulation and Experimental Results

Several PLECS simulations have been run to demonstrate the effectiveness of the proposed controllers when a DAB converter is driving an inverter. For this simulation, the inverter is assumed to be ideal. The base case is a unity-power-factor (resistive) load. System parameters are given in Tables I–V. Simulation results of all three methods, PI-only, PI plus feedforward control, and PI-R control, are given in the following figures. Four simulation cases are compared: PI-only with rated bus capacitance [see Fig. 15(a)], PI-only with four times larger bus capacitance [see

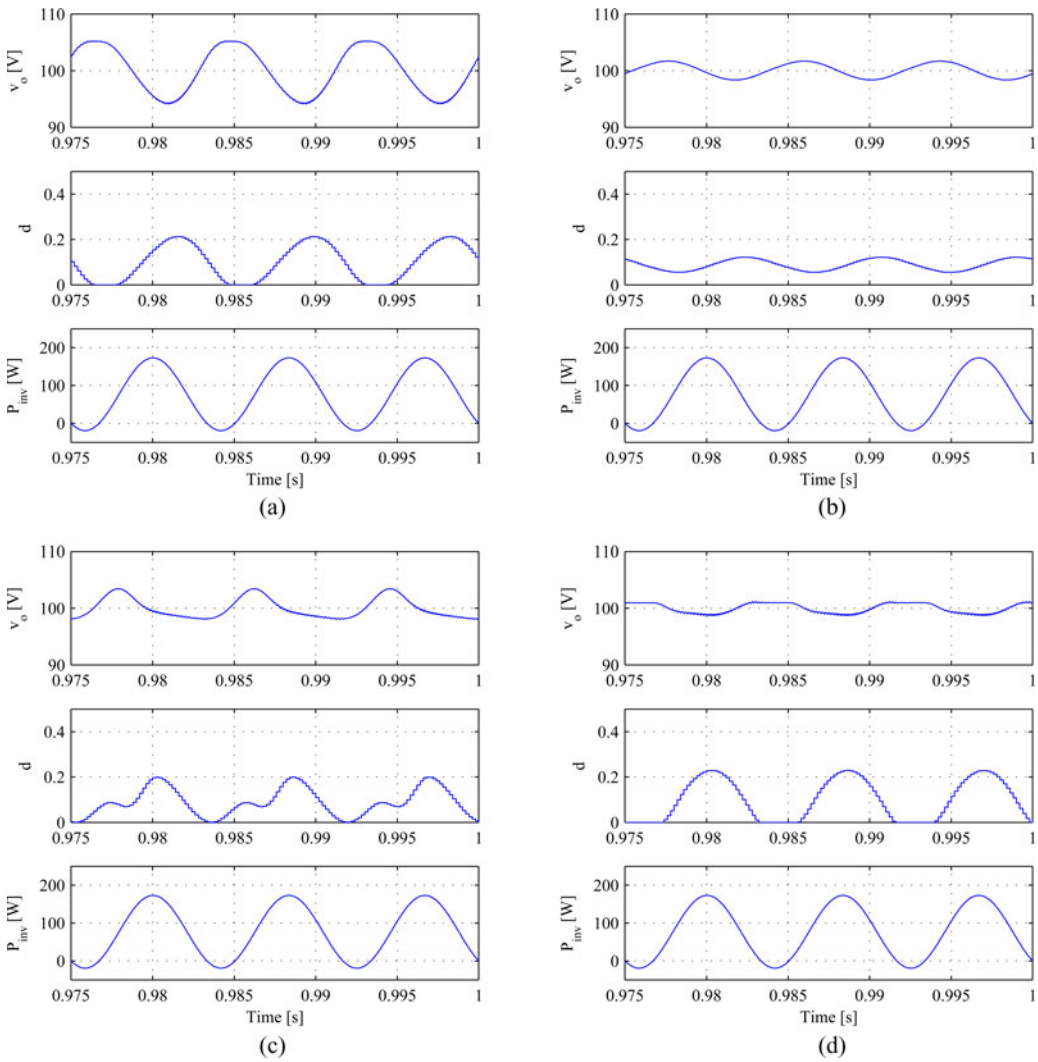

Fig. 17. Simulation Results. From top to bottom within a set: output voltage of DAB converter (V), duty ratio of DAB converter, output power of inverter (W). Load is $30 + j22.6\,\Omega$. (a) PI-only Control. (b) PI-only Control with four times capacitor. (c) PI-Feedforward Control. (d) PI-R Control.

Fig. 15(b)], PI with Feedforward with rated bus capacitance [see Fig. 15(c)], and PI-R control with rated bus capacitance [see Fig. 15(d)].

In the basic configuration with PI only control, the output voltage ripple is approximately 20 V, as shown in Fig. 15(a). Because of low loop gain and high output impedance at 120 Hz, the middle trace, duty ratio, is lagging the output voltage. The hardware solution is to increase bus capacitance by a factor of four, which reduces bus voltage ripple by a corresponding factor of four, as shown in Fig. 15(b).

If instead the bus capacitance remains at the nominal value and the controller is improved, a similar improvement in ripple may be achieved. Both feedforward [see Fig. 15(c)] and PI-R [see Fig. 15(d)] controllers achieve similar results. In both cases, the duty ratio variation is 180° out of phase with the output voltage ripple, so that the primary side source may supply the power ripple.

Although both feedforward and PI-R controllers achieve similar steady-state performance with resistive loads, they differ in transient performance and in their handling of nonunity-power-factor loads. For Fig. 16(a)–(d), the load is resistive but is stepped from $60[$ to $30\,\Omega$ at $t = 0.4\,\mathrm{s}$. The feedforward method nearly replicates the PI control performance. However, the PI-R controller has additional poles and zeros and a somewhat reduced phase margin, so the transient response in Fig. 16(d) exhibits more undershoot and longer settling time.

The advantage of a PI-R controller is robustness to power factor variation. For Fig. 17(a)– (d), the load is still linear but is inductive, $30 + j22.6\,\Omega = 37.6\angle 37^\circ\Omega$. The active power is reduced, so the ripple in general is lower than in the previous simulations. However, the ripple voltage for the case with a PI-R controller is nearly identical to the case with a PI control and four times bus capacitance, whereas the feedforward controller results in nearly twice the ripple. Direct comparison of just output voltage ripple is given in Fig. 18. To make an effective feedforward controller, the duty ratio ripple must be in phase with the active power ripple of the load, which is somewhat more challenging than synchronizing to the inverter output voltage.

The only case where the hardware solution is clearly advantageous is when the load is nonlinear. If the inverter is ideal

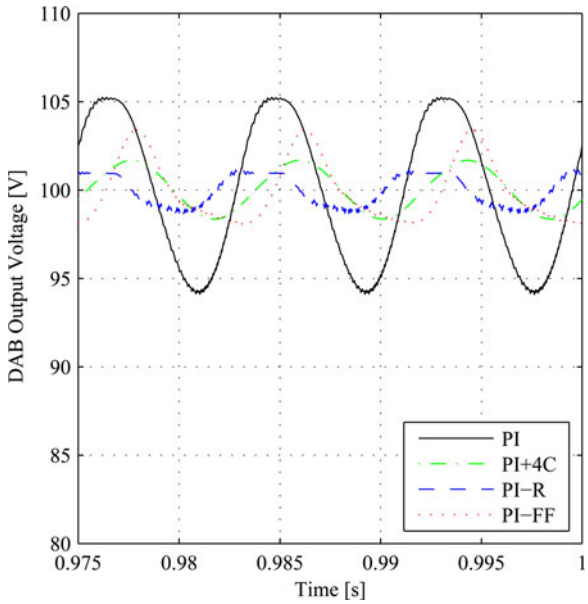

Fig. 18. Simulation Results. Comparison of just DAB output voltage with a load of $30 + j22.6\,\Omega$. "PI+4C" refers to a PI only controller with four times the nominal output capacitance.

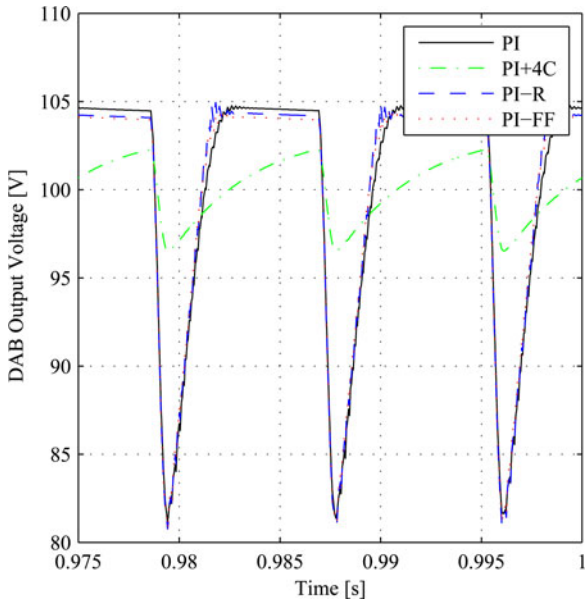

Fig. 19. Simulation Results. Comparison of just DAB output voltage with rectifier load consisting of $60\,\Omega$ in parallel with 3300μF. "PI+4C" refers to a PI only controller with four times the nominal output capacitance.

and is driving a rectifier load, the power demand will be narrow spikes. None of the controllers has adequate bandwidth to accommodate this type of load, so a larger capacitance is needed. Fig. 19 compares output voltage ripple for the four cases.

Fig. 20 shows the diagram of experimental setup. Output voltage of the DAB converter is sampled by an operational amplifier circuit and the on-chip analog-to-digital converter of the TMS320F28335. LPFs are used as an antialias filter for digital implementation of controllers. Feedback control algorithms, configurable to be PI-only, PI-Feedforward, or PI-R control, are

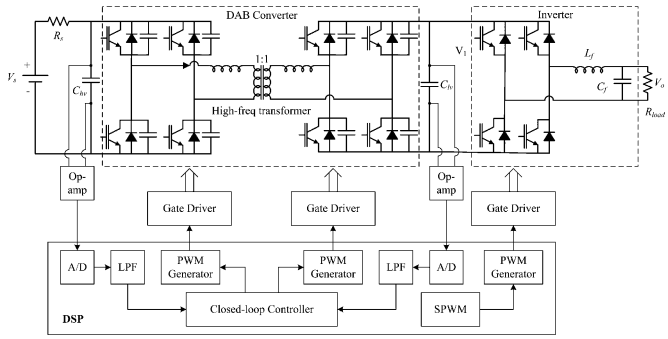

Fig. 20. Experimental hardware diagram.

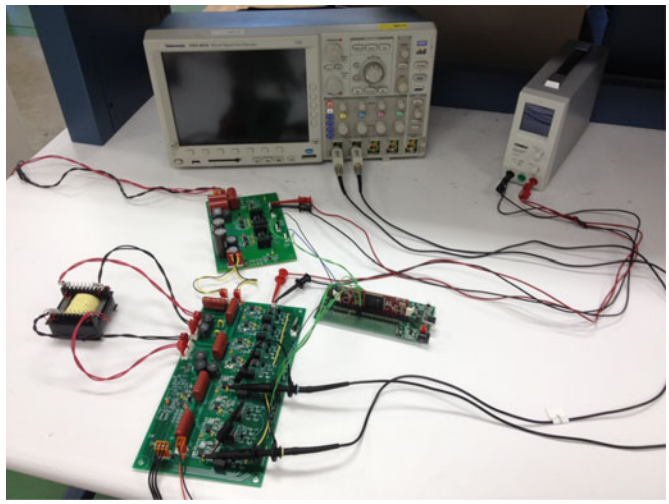

Fig. 21. Picture of experimental hardware.

programmed in the interrupt service routine of the DSP chip. The outputs of the feedback controller are fed to the on-chip PWM generator. The PWM signals are sent to gate drivers to turn-on/turn-off the power IGBTs. Fig. 21 shows a picture of the experimental setup, which consists of a DAB converter circuit board, an inverter circuit board, and a DSP development board manufactured by TI. Experimental results are given in Fig. 22(a)–(d).

Fig. 22(a) and (b) shows the experimental results of using the PI-only control scheme, when the output capacitance of the DAB converter is set to 200 μF (the rated value) and to 800 μF (four times of the rated value). The larger capacitor bank, which reduces the output impedance of a DAB converter, obviously reduces the ripple in DAB converter's output voltage (channel 2) caused by the 120 Hz current by the single-phase inverter. The transformer current of the DAB converter (channel 4) also indicates how high the loop gain is at 120 Hz and how the feedback controller tracks the error at 120 Hz. When the phase-shift ratio of a DAB converter tracks the output power ripple cause the downstream inverter, there would be a 120 Hz envelope in the resulting transformer current. Comparing the waveforms of channel 4 in Fig. 22(a) and (b), the 120 Hz envelope is more observable for the first case. For the same controller parameters, high output capacitance slows down the feedback loop. The

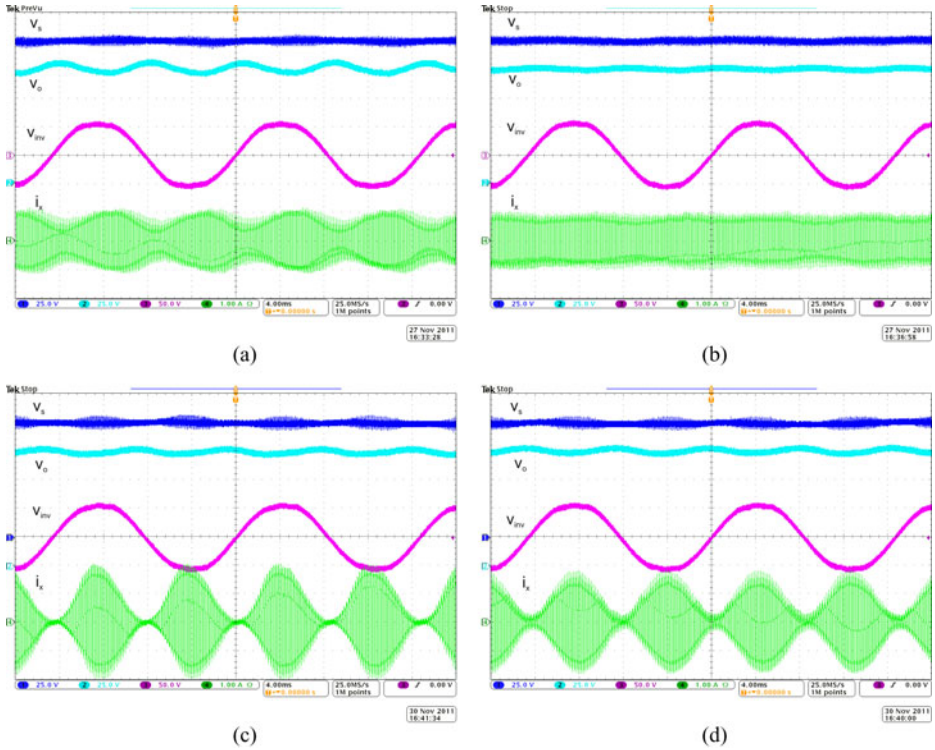

Fig. 22. Experimental Results. From top to bottom: Input Voltage of DAB Converter (V), Output Voltage of DAB Converter (V), Output Voltage of Inverter (V), Transformer Current of DAB Converter (A). 4ms/div. (a) PI-only Control. (b) PI-only Control with four times capacitor. (c) PI-Feedforward Control. (d) PI-R Control.

reason for low voltage ripple at the dc bus is simply that a larger capacitor can absorb more ripple current.

Fig. 22(c) shows the experimental results of using the PI-Feedforward control scheme. Voltage ripple reduces compared to Fig. 22(a). However, contrary to the case in Fig. 22(b), this is achieved not by increasing output capacitance, but by providing the DAB converter with the ability to track 120 Hz ripple power. Such ability is indicated by the 120 Hz envelope of the transformer current. When the output voltage of inverter approaches its peak (either positive peak or negative peak), the instantaneous power is also approaching its peak. As a result, the DAB converter supplies higher current to its load, the inverter. On the other hand, when an output voltage of the inverter is crossing zero, the instantaneous power is approaching zero. Therefore, the DAB converter also supply a near-zero current. This confirms that the DAB converter has the ability to track 120 Hz ripple power, enabled by feedforward.

Fig. 22(d) shows the experimental results of using the PI-R control scheme. Similar to Fig. 22(c), lower voltage ripple is observed without using larger capacitor. The 120 Hz envelope of the transformer current also confirms the the ability to track second-order ripple power. However, such ability is enabled not by feedforward, but by adding an additional R controller. This approach is more flexible and accommodates changing load magnitude and power factor.

VI. Conclusion

In the multistage configuration of an SST, a dc–dc DAB converter drives a single-phase dc–ac inverter. The cascaded connection of power converters poses a challenge for the closed-loop controller design. A single-phase inverter has significant second-order (120 Hz) harmonic current in its input side. A conventional PI controller has limited bandwidth at 120 Hz because of the relatively low switching frequency of the DAB converter. What is more, simply increasing switching frequency would not result in higher bandwidth. Two control methods are proposed to solve the aforementioned challenge without using a large dc bus capacitor between the DAB converter and the inverter. The first method uses the feedforward information from the inverter, while the second method adds an R controller to the feedback loop. Bode plot analysis of the loop gain and the closed-loop output impedance of DAB converters is used to study the limitation of PI controller and the effect of adding an R controller. Simulation and experimental results confirm the effectiveness of the proposed methods. The PI-R controller is more robust to changing load power factor, whereas the feedforward method provides better transient response. Both achieve ripple reduction similar to increasing bus capacitance by a factor of four.

References

[1] A. Huang, M. Crow, G. Heydt, J. Zheng, and S. Dale, "The future renewable electric energy delivery and management (freedm) system: The energy internet," *Proc. IEEE*, vol. 99, no. 1, pp. 133–148, Jan. 2011.

[2] E. R. Ronan, S. D. Sudhoff, S. F. Glover, and D. L. Galloway, "A power electronic-based distribution transformer," *IEEE Power Eng. Rev.*, vol. 22, no. 3, pp. 61–61, Mar. 2002.

[3] S. Bhattacharya, T. Zhao, G. Wang, S. Dutta, S. Baek, Y. Du, B. Parkhideh, X. Zhou, and A. Q. Huang, "Design and development of generation-i silicon based solid state transformer," in *Proc. IEEE Appl. Power Electron. Conf. Expo.*, Feb. 2010, pp. 1666–1673.

[4] H. Qin and J. Kimball, "A comparative efficiency study of silicon-based solid state transformers," in *Proc. IEEE Energ. Convers. Congr. Expo.*, Sep. 2010, pp. 1458–1463.
[5] D. Holmes, T. Lipo, B. McGrath, and W. Kong, "Optimized design of stationary frame three phase ac current regulators," *IEEE Trans. Power Electron.*, vol. 24, no. 11, pp. 2417–2426, Nov. 2009.
[6] J. Hwang, P. Lehn, and M. Winkelnkemper, "A generalized class of stationary frame-current controllers for grid-connected AC–DC converters," *IEEE Trans. Power Del.*, vol. 25, no. 4, pp. 2742–2751, Oct. 2010.
[7] D. Dong, T. Thacker, R. Burgos, D. Boroyevich, and F. Wang, "On zero steady-state error voltage control of single-phase PWM inverters with different load-types," *IEEE Trans. Power Electron.*, vol. 26, no. 11, pp. 3285–3297, Nov. 2011.
[8] W. Zhao, D. D.-C. Lu, and V. G. Agelidis, "Current control of grid-connected boost inverter with zero steady-state error," *IEEE Trans. Power Electron.*, vol. 26, no. 10, pp. 2825–2834, Oct. 2011.
[9] V.-T. Phan and H.-H. Lee, "Control strategy for harmonic elimination in stand-alone DFIG applications with nonlinear loads," *IEEE Trans. Power Electron.*, vol. 26, no. 9, pp. 2662–2675, Sep. 2011.
[10] P. Loh, Y. Tang, F. Blaabjerg, and P. Wang, "Mixed-frame and stationary-frame repetitive control schemes for compensating typical load and grid harmonics," *IET Power Electron.*, vol. 4, no. 2, pp. 218–226, Feb. 2011.
[11] H. Nian and R. Zeng, "Improved control strategy for stand-alone distributed generation system under unbalanced and non-linear loads," *IET Renewable Power Generat.*, vol. 5, no. 5, pp. 323–331, Sep. 2011.
[12] J. Hu and Y. He, "Modeling and control of grid-connected voltage-sourced converters under generalized unbalanced operation conditions," *IEEE Trans. Energy Convers.*, vol. 23, no. 3, pp. 903–913, Sep. 2008.
[13] S. Yang, Q. Lei, F. Peng, and Z. Qian, "A robust control scheme for grid-connected voltage-source inverters," *IEEE Trans. Ind. Electron.*, vol. 58, no. 1, pp. 202–212, Jan. 2011.
[14] A. Hasanzadeh, O. Onar, H. Mokhtari, and A. Khaligh, "A proportional-resonant controller-based wireless control strategy with a reduced number of sensors for parallel-operated UPSs," *IEEE Trans. Power Del.*, vol. 25, no. 1, pp. 468–478, Jan. 2010.
[15] A. Timbus, M. Liserre, R. Teodorescu, P. Rodriguez, and F. Blaabjerg, "Evaluation of current controllers for distributed power generation systems," *IEEE Trans. Power Electron.*, vol. 24, no. 3, pp. 654–664, Mar. 2009.
[16] Y. W. Li, F. Blaabjerg, D. Vilathgamuwa, and P. C. Loh, "Design and comparison of high performance stationary-frame controllers for DVR implementation," *IEEE Trans. Power Electron.*, vol. 22, no. 2, pp. 602–612, Mar. 2007.
[17] A. Yepes, F. Freijedo, O. Lopez, and J. Doval-Gandoy, "Analysis and design of resonant current controllers for voltage-source converters by means of Nyquist diagrams and sensitivity function," *IEEE Trans. Ind. Electron.*, vol. 58, no. 11, pp. 5231–5250, Nov. 2011.
[18] A. Roslan, K. Ahmed, S. Finney, and B. Williams, "Improved instantaneous average current-sharing control scheme for parallel-connected inverter considering line impedance impact in microgrid networks," *IEEE Trans. Power Electron.*, vol. 26, no. 3, pp. 702–716, Mar. 2011.
[19] P. Mattavelli, "Synchronous-frame harmonic control for high-performance ac power supplies," *IEEE Trans. Ind. Appl.*, vol. 37, no. 3, pp. 864–872, May/Jun. 2001.
[20] M. Newman and D. Holmes, "Delta operator digital filters for high performance inverter applications," *IEEE Trans. Power Electron.*, vol. 18, no. 1, pp. 447–454, Jan. 2003.
[21] A. Jain and R. Ayyanar, "PWM control of dual active bridge: Comprehensive analysis and experimental verification," *IEEE Trans. Power Electron.*, vol. 26, no. 4, pp. 1215–1227, Apr. 2011.
[22] Y. Jin, Q. Song, W. Liu, and W. Sun, "Cascaded battery energy storage system based on dual active bridges and a common DC bus," in *Proc. Int. Power Energy Conf.*, 2010, pp. 1019–1024.
[23] G. Oggier, G. Garci anda, and A. Oliva, "Modulation strategy to operate the dual active bridge DC-DC converter under soft switching in the whole operating range," *IEEE Trans. Power Electron.*, vol. 26, no. 4, pp. 1228–1236, Apr. 2011.
[24] K. Wu, C. W. de Silva, and W. G. Dunford, "Stability analysis of isolated bidirectional dual active full-bridge DC–DC converter with triple phase-shift control," *IEEE Trans. Power Electron.*, vol. 27, no. 4, pp. 2007–2017, Apr. 2012.
[25] B. Zhao, Q. Song, and W. Liu, "Power characterization of isolated bidirectional dual-active-bridge DC–DC converter with dual-phase-shift control," *IEEE Trans. Power Electron.*, vol. 27, no. 9, pp. 4172–4176, Sep. 2012.
[26] D. Costinett, D. Maksimovic, and R. Zane, "Design and control for high efficiency in high step-down dual active bridge converters operating at high switching frequency," *IEEE Trans. Power Electron.*, vol. 28, no. 8, pp. 3931–3940, Aug. 2013.
[27] L. D. Watson, J. W. Kimball, and S. Atcitty, "Linear single phase inverter model for battery energy storage system evaluation and controller design," in *Proc. IEEE Appl. Power Electron. Conf.*, Feb. 2012, pp. 1861–1867.
[28] H. Qin and J. W. Kimball, "Generalized average modeling of dual active bridge DC–DC converter," *IEEE Trans. Power Electron.*, vol. 27, no. 4, pp. 2078–2084, Apr. 2011.
[29] H. K. Krishnamurthy and R. Ayyanar, "Building block converter module for universal (AC–DC, DC–AC, DC–DC) fully modular power conversion architecture," in *Proc. IEEE Power Electron. Spec. Conf.*, Jun. 2007, pp. 483–489.
[30] B. Hua, C. C. Mi, and S. Gargies, "The short-time-scale transient processes in high-voltage and high-power isolated bidirectional DC–DC converters," *IEEE Trans. Power Electron.*, vol. 23, no. 6, pp. 2648–2656, Jun. 2008.
[31] H. Bai, Z. Nie, and C. C. Mi, "Experimental comparison of traditional phase-shift, dual-phase-shift, and model-based control of isolated bidirectional DC–DC converters," *IEEE Trans. Power Electron.*, vol. 25, no. 6, pp. 1444–1449, Jun. 2010.
[32] F. Krismer and J. W. Kolar, "Accurate small-signal model for the digital control of an automotive bidirectional dual active bridge," *IEEE Trans. Power Electron.*, vol. 24, no. 12, pp. 2756–2768, Dec. 2009.
[33] C. Zhao, S. D. Round, and J. W. Kolar, "Full-order averaging modelling of zero-voltage-switching phase-shift bidirectional DC–DC converters," *IET Power Electron.*, vol. 3, no. 3, pp. 400–410, Mar. 2010.
[34] C.-T. Chen, *Linear System Theory and Design*. London, U.K.: Oxford Univ., Press, 1998.

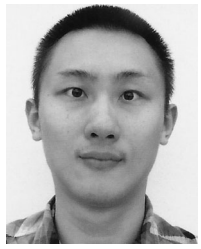

Hengsi Qin received the B.S. and M.S. degrees in electrical engineering from Central South University, Changsha, Hunan, China, in 2005 and 2008, respectively. He received the Ph.D. degree in electrical engineering from the Department of Electrical and Computer Engineering, Missouri University of Science and Technology (Missouri S&T), Rolla MO, in 2012.

He is currently a Senior Engineer at SolarBridge Technologies, Austin TX, USA, working on photovoltaic microinverter for ACPV modules. His current research interests include the analysis, design, control, and optimization of power electronic converters in renewable electric power grid.

Jonathan W. Kimball (M' 96–SM' 05) received the B.S. degree in electrical and computer engineering from Carnegie Mellon University, Pittsburgh, PA, USA, in 1994, and the M.S. degree in electrical engineering and the Ph.D. degree in electrical and computer engineering from the University of Illinois at Urbana- Champaign, Urbana-Champaign, IL, USA, in 1996 and 2007.

From 1996 to 1998, he was with Motorola, Phoenix, AZ, USA, where he was engaged in designing insulated gate bipolar transistor modules for industrial applications. He then joined Baldor Electric, Fort Smith, AR, where he designed industrial adjustable-speed drives ranging 1–150 hp. In 2003, he joined the University of Illinois as a Research Engineer, where he later became a Senior Research Engineer. In 2003, he cofounded SmartSpark Energy Systems, Inc., Champaign, IL, where he was the Vice President of Engineering. In 2008, he joined Missouri University of Science and Technology (Missouri S&T), Rolla, where he is currently an Assistant Professor.

Dr. Kimball is a Member of Eta Kappa Nu, Tau Beta Pi, and Phi Kappa Phi. He is a licensed Professional Engineer in the State of Illinois.